

DRAFT VERSION FEBRUARY 15, 2018

Preprint typeset using L^AT_EX style AASTeX6 v. 1.0

X-RAY FLARE OSCILLATIONS TRACK PLASMA SLOSHING ALONG STAR-DISK
MAGNETIC TUBES IN ORION STAR-FORMING REGION

FABIO REALE¹

Dipartimento di Fisica & Chimica, Università di Palermo, Piazza del Parlamento 1, 90134 Palermo, Italy;

fabio.reale@unipa.it

JAVIER LOPEZ-SANTIAGO

Department of Signal Theory & Communications, Universidad Carlos III de Madrid, Avda. de la Universidad 30,

Leganes, 28911 Madrid, Spain

ETTORE FLACCOMIO, ANTONINO PETRALIA, SALVATORE SCIORTINO

INAF-Osservatorio Astronomico di Palermo, Piazza del Parlamento 1, 90134 Palermo, Italy

¹and INAF-Osservatorio Astronomico di Palermo, Piazza del Parlamento 1, 90134 Palermo, Italy

Abstract

Pulsing X-ray emission tracks the plasma echo traveling in an extremely long magnetic tube that flares in an Orion Pre-Main Sequence (PMS) star. On the Sun, flares last from minutes to a few hours and the longest-lasting typically involve arcades of closed magnetic tubes. Long-lasting X-ray flares are observed in PMS stars. Large-amplitude

arXiv:1802.05093v1 [astro-ph.SR] 14 Feb 2018

($\sim 20\%$) long-period (~ 3 hours) pulsations are detected in the light curve of day-long flares observed by the *Advanced CCD Imaging Spectrometer* (ACIS) on-board *Chandra* from PMS stars in the Orion cluster. Detailed hydrodynamic modeling of two flares observed on V772 Ori and OW Ori shows that these pulsations may track the sloshing of plasma along a single long magnetic tube, triggered by a sufficiently short (~ 1 hour) heat pulse. These magnetic tubes are as long (≥ 20 solar radii) as to connect the star with the surrounding disk.

Keywords: Sun: activity — Sun: corona — Sun: flares — stars: flare — stars: coronae

1. INTRODUCTION

Close to the end of their formation, stars are surrounded by a gas and dust disk, from which planets form. Magnetic fields are known to play a key role in the star-disk system (Johns-Krull 2014). It is believed that the inner regions of the disk are significantly ionized by the stellar radiation and that accreting material flows along magnetic channels that connect the disk to the star (Koenigl 1991). Very long and intense X-ray flares in star forming regions might occur in such long channels (Favata et al. 2005), but this is highly debated (Getman et al. 2008). These flux tubes might resemble those observed in the solar corona and diagnosed in the stellar coronae, but on a much larger scale. On the Sun we see the so-called coronal loops on the scale of several thousand kilometers in active regions, but some faint large-scale structures can extend up to $\sim 1 R_{\odot}$ (Reale 2014). Most solar flares occur in active region loops, but the long-lasting ones can involve more and more loops aligned in arcades. The other stars are so distant that we cannot resolve the flaring regions, but it is supposed that they occur in loops and even in arcades. Whereas the duration of solar flares typically ranges from few minutes to several hours, stellar flares can be very intense, more than the solar bolometric luminosity, and long-lasting, more than one day, in very active stars. Several of such gigantic coronal

flares have been surveyed in star-forming regions (Favata et al. 2005) and where they occur is a big question. Magnetic instabilities in flux tubes were proposed as the origin of the flaring activity also in T Tauri stars (Birk 1998; Birk et al. 2000), and long-lasting stellar flares might be expected to involve loop arcades (Getman et al. 2008) as on the Sun. In the long-lasting solar flares, the duration is mainly due to the progressive involvement of more and similar loops, and therefore it is not directly linked to the size of the flaring structures. This might be the case also for the giant stellar flares. However, if a single stellar loop were flaring, the cooling time of the confined plasma would be proportional to the loop length (Serio et al. 1991; Reale 2014), and day-long flares would correspond to giant loops, as long as possibly connecting the star with the disk (Hartmann et al. 2016). There are ways to distinguish between a pure cooling in a single loop and a decay only due to progressive reduction of the energy release in a loop arcade (Reale et al. 1997), but the arguments are debated and the uncertainties are large (Getman et al. 2008). Several studies (Favata et al. 2005; Giardino et al. 2007) find results compatible with long magnetic channels in PMS stars, but the derivation of the loop length is based on the assumption of a flare occurring in a single loop (Reale 2007).

Different diagnostics independent of flare cooling would be desirable to solve this ambiguity between long and arcade flaring structures. A new way would be to detect and study brightness wave fronts traveling along the magnetic flux tubes. These might prompt periodic pulsations in the flare light curves, whose period would track back to the length of the wave guide. This concept has been pursued recently in a general hydrodynamic modeling framework and used as a new tool to diagnose the duration of the flare heat pulse (Reale 2016). Periodic pulsations have been detected in the light curves of several stellar X-ray flares (Mitra-Kraev et al. 2005; Welsh et al. 2006; Pandey & Srivastava 2009; López-Santiago et al. 2016), but generally not linked to the size of the flaring structure.

In this work, we show that the modulated light curve of long flares observed in the soft X-rays with

Chandra/ACIS on young stars (V772 Ori, OW Ori) in the Orion star-forming region is well explained by flaring plasma sloshing back and forth inside a single flaring magnetic tube, that is several stellar radii long. Such long structures can be hardly mapped as semicircular loops, and in the following we will address them more generally as magnetic flux tubes. Both stars are surrounded by a disk and have been observed to be active accretors (see Section 2 for more details). The length of the flaring tubes analysed in this work is enough to suggest a connection between the star and the accretion disk.

Section 2 describes the data, in Section 3 they are modelled and the results discussed in Section 4.

2. THE DATA ANALYSIS

For this work, we use data from the Chandra Orion Ultradeep Project (COUP, [Getman et al. 2005b](#)). We focus on V772 Ori (COUP 43) and on OW Ori (COUP 1608), two young M stars that underwent strong, long-duration flares during the observations ([Favata et al. 2005](#)).

V772 Ori ($A_V = 1.18$, [Aarnio et al. 2010](#)) is an M1.5 star ([Hillenbrand et al. 2013](#)) with $M = 0.4 M_\odot$ and radius $R_\star = 2.9 R_\odot$ ([Getman et al. 2005a](#)). It was listed as a candidate double-lined spectroscopic binary ([Rhode et al. 2001](#)), still not confirmed ([Biazzo et al. 2009](#)). For this star a photometric period $P = 1.69 \pm 0.02$ days was measured and it was classified as an accretor based on its intense H_α emission line ([Stassun et al. 1999](#)). Equivalent widths were determined for H_α and Li I from high-resolution ($R > 30000$) optical spectra ([Stassun et al. 1999](#)). The $EW(H_\alpha)$ was corrected for possible narrow nebular emission line. The results were: $EW(\text{Li I}) = 260 \text{ m}\text{\AA}$, $EW(H_\alpha) = 43.4 \text{ \AA}$ (see Fig.7 in [Stassun et al. 1999](#)). Radio VLA fluxes ($F(4.5\text{GHz}) = 0.88 \pm 0.27 \text{ mJy}$ and $F(7.5\text{GHz}) = 0.67 \pm 0.18 \text{ mJy}$) also confirm the presence of a disk around this star ([Kounkel et al. 2014](#)).

The total COUP light curve shows two flares for this star, one after the other ([Favata et al. 2005](#)). We study the second one, which is observed in its entirety, while for the first one we only see part of

the decay. There is no particular evidence that one flare is related to the other, so we will assume they are not.

OW Ori is a well-known M0.5e classical T Tauri star located inside the Orion Nebula Cluster (Hillenbrand 1997), with mass $M=0.48 M_{\odot}$ and radius $R_{\star}=1.77 R_{\odot}$ (Getman et al. 2005b). Infrared excesses $\Delta(I - K) = 1.41$ (Hillenbrand et al. 1998) and $\Delta(H - K) = 0.13$ (Getman et al. 2008) were derived. Both are indicative of an accretion disk. The extinction towards OW Ori is $A_V = 0.25$ mag (Aarnio et al. 2010). It was derived (Aarnio et al. 2010) a dust destruction radius in the accretion disk $R_{\text{dust}} = 10 R_{\odot}$, close to the co-rotation radius ($R_{\text{cor}} = 8.6 R_{\odot}$) (Getman et al. 2008). These results indicate the presence of an inner disk. The rotational period of the star is $P = 4.21$ days (Rhode et al. 2001).

The X-ray characteristics of both flares were studied previously (Favata et al. 2005; Getman et al. 2008). We focus our attention on the oscillation patterns in the X-ray light curve revealed by the *Chandra X-ray Observatory* (CXO) during the stellar flares. Data reduction was performed within the COUP. Details can be found in Getman et al. (2005b). The Chandra dither has negligible effect on the sources analysed in this work. During the analysis performed for López-Santiago et al. (2016), we found the ~ 700 s pattern due to Chandras dither in some stars of the COUP close to a gap between chips. However, this is not the case for COUP 43 or COUP 1608 (Getman et al. 2005b), whose large off-axis angle makes the counts distribution large compared to the area of the dead columns.

Spectral analysis for the flare of V772 Ori was carried out independently in two works (Favata et al. 2005; Getman et al. 2008), using different methods. Favata et al. (2005) performed a time-resolved spectral analysis by extracting X-ray spectra in time intervals selected through a maximum likelihood algorithm, with the pre-imposed condition of having enough photon statistics for spectral analysis. Spectral fits of the resulting X-ray spectra were then done using the XSPEC package assuming the

MEKAL spectral emissivity model for coronal equilibrium plasma. The obtained plasma characteristics in each time interval are mean values of the actual plasma parameters during that time period. The spectral range analyzed in this work was $0.5 - 7$ keV. A single thermal component was assumed, with the global abundance fixed to $0.3 Z_{\odot}$ (Favata et al. 2005). The absorbing column density was left free to vary. With these constraints, a temperature of 58 MK was found for the flaring plasma, corresponding to a peak temperature $T_{peak} = 142$ MK (Favata et al. 2005; Reale et al. 2007). The peak emission measure is $EM_{peak} \approx 10^{54} \text{ cm}^{-3}$ and the absorption column density is $\log N_H[\text{cm}^{-2}] \approx 21$.

Instead, Getman et al. (2008) based their analysis on the method of adaptively smoothed median energy (MASME). In practice, they analyzed the median energy of photons during the flare and the count-rate instead of performing a time-resolved spectral fitting. Despite the two works obtain different results for the peak temperature and emission measure for some stars of the COUP, this is not the case for our target (V772 Ori). Getman et al. (2008) determined $EM_{peak} = 1.2 \times 10^{54} \text{ cm}^{-3}$ and $T_{obs} = 59$ MK, which are very close to the values derived by Favata et al. (2005).

The raw light curve is actually dominated by low count statistics ($\sim 0.03 - 0.04$ cts/s) and the presence of any periodic signal is hardly detectable from direct inspection and with no data interpolation. To reveal oscillations in the light curve of V772 Ori in an objective way, we follow the procedure applied to other COUP flares (López-Santiago et al. 2016). Firstly, we select events for the X-ray source only in the time period of the flare and generate a light curve with temporal resolution 100 seconds. Then, this flare light curve is normalized using a moving average. With this procedure, the general shape of the flare is subtracted. The normalized flare light curve is then convolved with a Morlet function, which has the advantage of preserving information in the time domain (López-Santiago et al. 2016). The result of the convolution is a 2D power spectrum: the time-frequency representation of the light curve. If any oscillation is present in the original dataset,

it is revealed as a feature (peak) in the wavelet power spectrum. The significance of such peaks is determined by generating confidence levels. To do this, a background noise model must be assumed. This background noise is derived from the univariate lag-1 autoregressive, or Markov process. Details on the methodology are given in [Torrence & Compo \(1998\)](#) and summarized in [López-Santiago et al. \(2016\)](#). In our work, we assume *red noise* instead of the white noise background typically used in the literature. The assumption of white noise for deriving confidence levels in a flare light curve usually overestimates the significance of low-frequency patterns and underestimates the significance of high-frequency patterns. The time binning of 100 s is not an integral multiple of the ACIS frame time for these observations, i.e., 3.14104 s, but this produces no significant aliasing in our results. We also repeated our analysis with other sampling periods, i.e., 50 s, 30 s, 5 s, and obtained the same results.

This work addresses the detection of pulsations with the longest duration, which may be evidence of very long loops. We consider as actual (long) pulsations only those features lasting for at least three times the period at which they are revealed in the power spectrum. [Figure 1](#) presents the result of the wavelet transform for the flare underwent by the star V772 Ori during the COUP observations. The upper panel shows the light curve analyzed in this work. The line overplotted is the moving average (bin = 15 ks). The bottom panel shows the wavelet power spectrum. Contours are for the confidence levels 67% (dotted line), 95% (dashed line) and 99% (continuous line), assuming red noise as the background signal. The power spectrum reveals a significative persistent feature at period $P = 10 \pm 1$ ks (~ 3 hrs) over a time range of ~ 40 ks around the peak of the flare. This feature corresponds to a pulsation extending for approximately four periods, as actually shown in [Figure 2](#).

[Figure 2a](#) shows the observed light curve with a binning of 1200 s, replicated after slight shifts of 100 s (black solid line), and after smoothing with a Gaussian with $\sigma = 2000$ s (blue dashed line). Each binned light curve is noisy but the envelope of them provides a hint of the dips and cusps of

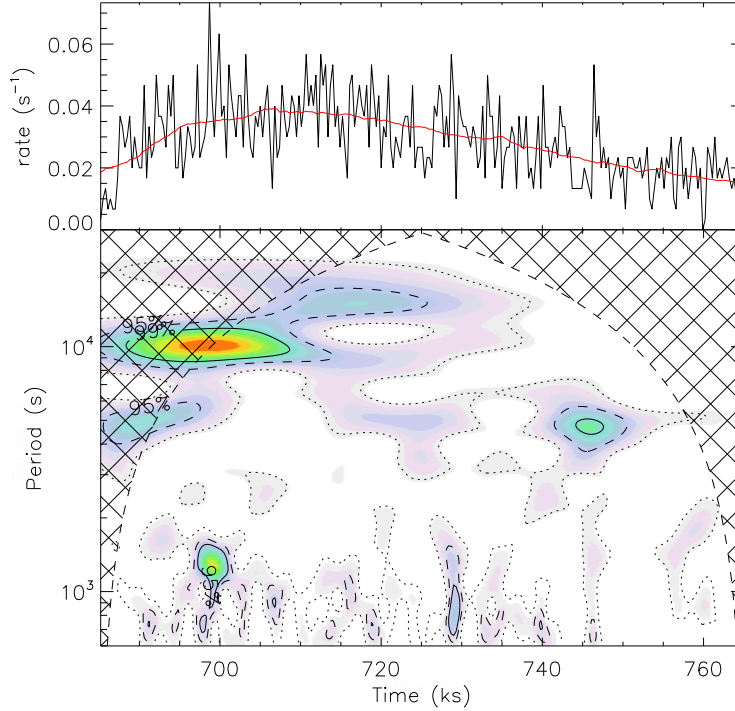
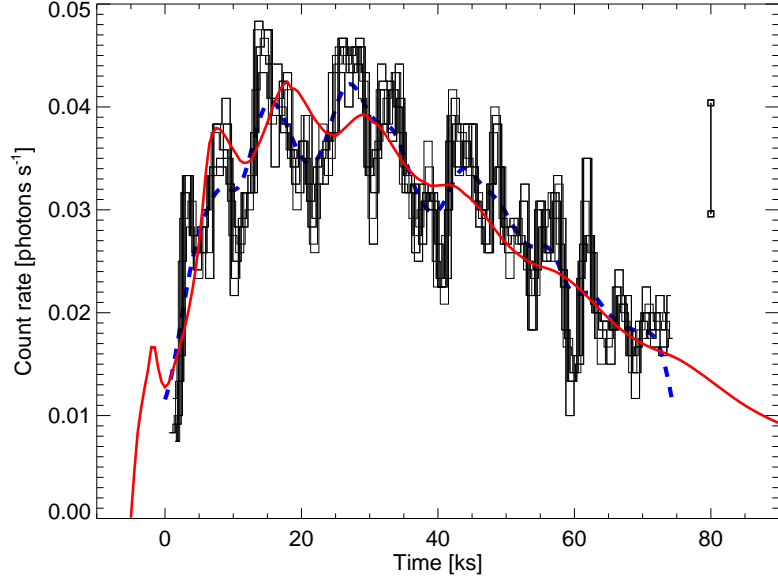


Figure 1. Flare light curve (upper panel) and wavelet power spectrum (bottom panel) for V772 Ori. The continuous line in the upper panel represents the moving average used to subtract the general shape of the flare. The contours in the bottom panel are confidence levels: continuous line is 99%, dashed line is 90% and dotted line is 67%. The hatched area is the cone of influence (COI), the region of the wavelet power spectrum in which edge effects become important.

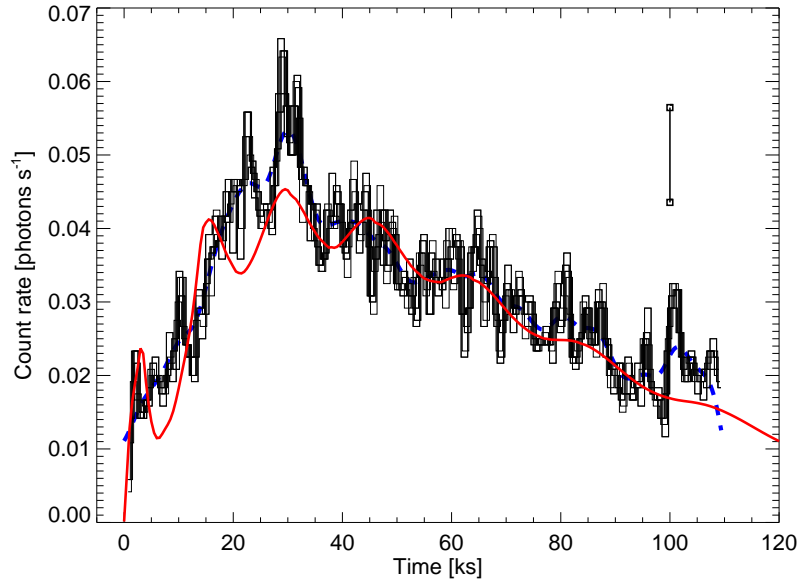
the oscillations. The smoothed light curve shows periodic pulsations with the period found with the wavelet analysis above. We point out that the detection of the oscillations is made from the light curve with the fine binning shown in Fig. 1.

A possible interaction between binary components certainly cannot explain the period of the observed oscillations: according to Kepler’s laws, the period is too short to be compatible with the orbital period of a possible binary, unless the system is very unlikely a contact binary.

For the flare on OW Ori, the wavelet analysis (López-Santiago et al. 2016) revealed a feature at $P \sim 10$ ks. The authors showed that this feature corresponds to an oscillation with amplitude $\geq 5\%$ of the flare intensity ($\Delta I/I \geq 0.05$). Figure 2b shows the related light curve, in the same format as



(a)



(b)

Figure 2. Flare light curves observed with Chandra/ACIS from (a) V772 Ori (COUP 43; Obs. ID 4374) and (b) OW Ori (COUP 1608; Obs. ID 4373), with a binning of 1200 s, each shifted by 100 s (black solid) and after smoothing with a Gaussian with $\sigma = 2000$ s (blue dashed). The observed light curves are compared to those obtained from respective hydrodynamic simulations of a flaring flux tube 20 and 30 R_{\odot} long and heat pulses of ~ 1 hour (red solid). The vertical bar on the right marks a typical data error bar.

for the flare of V772 Ori.

3. HYDRODYNAMIC MODELING

As in previous stellar flare modeling (Reale et al. 1988; Favata et al. 2005; Testa et al. 2007; Schmitt et al. 2008), we model the flaring plasma as confined inside a magnetic flux tube. The plasma is compressible and confined by the magnetic field and moves and transports energy along the field lines. The plasma evolution can then be described with a single-fluid one-dimensional hydrodynamic model where the coordinate is the distance along the tube. We assume that the tube is a closed coronal flux tube anchored at the footpoints. In a typical corona the footpoints are anchored at two different locations of the chromosphere/photosphere. In the case of a young star one of (or even both) the locations might be on the disk which might be as dense as a stellar chromosphere (Kastner et al. 2002; Telleschi et al. 2007; Argiroffi et al. 2007). The model is analogous to that used in Favata et al. (2005). The magnetic tube is assumed symmetric with respect to the middle, and we model only half of it. The gravity component along the flux tube is computed assuming a radius $R_* = 3R_\odot$ and a surface gravity $g_* = 0.1g_\odot$, typical of low-mass PMS objects (Favata et al. 2005). A fine tuning of these parameters is not important for the modeling because the plasma evolution is largely dominated by the heating and cooling processes and by the dynamics driven by the heat pulse (Bradshaw & Cargill 2010). In the following, we describe in detail the model for the flare on V772 Ori.

The length of the tube is mainly determined by the flare decay time which – for a closed flaring coronal magnetic flux tube starting from equilibrium conditions – scales as (Serio et al. 1991; Reale 2014):

$$\tau_d \approx 5 \frac{L_\odot}{\sqrt{T_6}} \quad (1)$$

where τ_d is in hours, T_6 is the flare maximum temperature in units of 10^6 K, L_\odot is the tube total length in units of solar radii (R_\odot). Since the thermal conduction is extremely efficient along the tube, we can estimate its maximum temperature from the scaling laws for static coronal loops (Rosner et al. 1978; Reale 2014), even if the tube is never close to an equilibrium during the flare. We obtain:

$$T_6 \sim 2.3 H_{-3}^{2/7} L_\odot^{5/21} \sim 180 \quad (2)$$

where H_{-3} is the heating rate per unit volume in units of 10^{-3} erg cm $^{-3}$ s $^{-1}$. Although the observed decay time is about 4 hours (Figure 2a) which, for this estimated temperature, corresponds to a length $L_\odot \sim 12$, after test simulations, we find that a tube length $L_\odot = 20$ matches better the observed light curve, i.e., the decay and the oscillation period.

We assume that there is plasma confined in this long tube before the flare. This plasma is much cooler and more tenuous than it gets during the flare, with a maximum temperature of 17 MK and a pressure of 2 dyn cm $^{-2}$ at the footpoints, similar to previous work (Favata et al. 2005). These initial conditions are kept steady and at equilibrium in the corona by a uniform heating of 3.5×10^{-5} erg cm $^{-3}$ s $^{-1}$. The tube atmosphere includes a relatively thick chromosphere at the footpoints which is described according to one standard model (Vernazza et al. 1981). In typical flare loop modeling the chromosphere has mainly the role of providing a mass reservoir for filling the flux tube with dense plasma (Reale 2014). So we assume that this model chromosphere is valid both for footpoints rooted on the stellar surface and on the disk. The flare is triggered in the tube atmosphere by suddenly releasing a powerful heat pulse, much stronger than the equilibrium heating mentioned above. The condition to trigger the plasma sloshing inside the magnetic tube, which determines the pulsations observed in the light curve, is that the duration of the heat pulse τ_H must be shorter than return sound crossing time along the tube τ_s at the peak of the flare (Reale 2016):

$$\tau_H < \tau_s \approx 1.5 \frac{L_\odot}{\sqrt{T_6}} \quad (3)$$

where τ_H and τ_s are in hours. The pulsation period is still the sound crossing time but taken during the flare decay, i.e., longer than τ_s , because in Equation (3) we should use quite a smaller temperature than the flare maximum temperature T_6 . On the other hand, since these flares, as many others observed in young stars, are very hot, reaching temperatures above 100 MK (Favata et al. 2005), according to Equation (3), a measured period of ~ 3 hours involves tube lengths $\geq 20R_\odot$. Moreover, since the decay time in Equation (1) scales as the sound crossing time in Equation (3), we will always see a similar number of pulsations in this and other analogous flares, i.e., about five-to-ten (Reale 2016).

With the maximum temperature T_6 derived in Eq.(2), from Eq.(3) we obtain $\tau_H < 2.5$ hrs. We obtain a very similar evolution with heat pulses with a duration of 3000-4000 s (≈ 1 hour), safely within the condition to trigger the plasma sloshing, and deposited in the corona either uniformly along the tube with an intensity of $0.1 \text{ erg cm}^{-3} \text{ s}^{-1}$, i.e. ~ 3000 times stronger than the equilibrium heating, or more concentrated toward the middle of the tube (a Gaussian with a width $\sigma_H = 10^{11}$ cm) and an intensity $0.5 \text{ erg cm}^{-3} \text{ s}^{-1}$. The heat distribution is not an important parameter because the thermal conduction is very efficient and levels out the temperature in a short time along the tube (Bradshaw & Cargill 2006).

We let the plasma confined in the tube evolve from the initial conditions above and under the action of the heat pulse above, by solving numerically the hydrodynamic equations for a compressible plasma. The equations and numerical model are described in previous works (Peres et al. 1982; Betta et al. 1997). The grid is adaptive with a maximum spatial resolution of 0.1 km. Figure 3 shows the evolution of some representative quantities for 120 ks, i.e., the temperature, density and pressure at

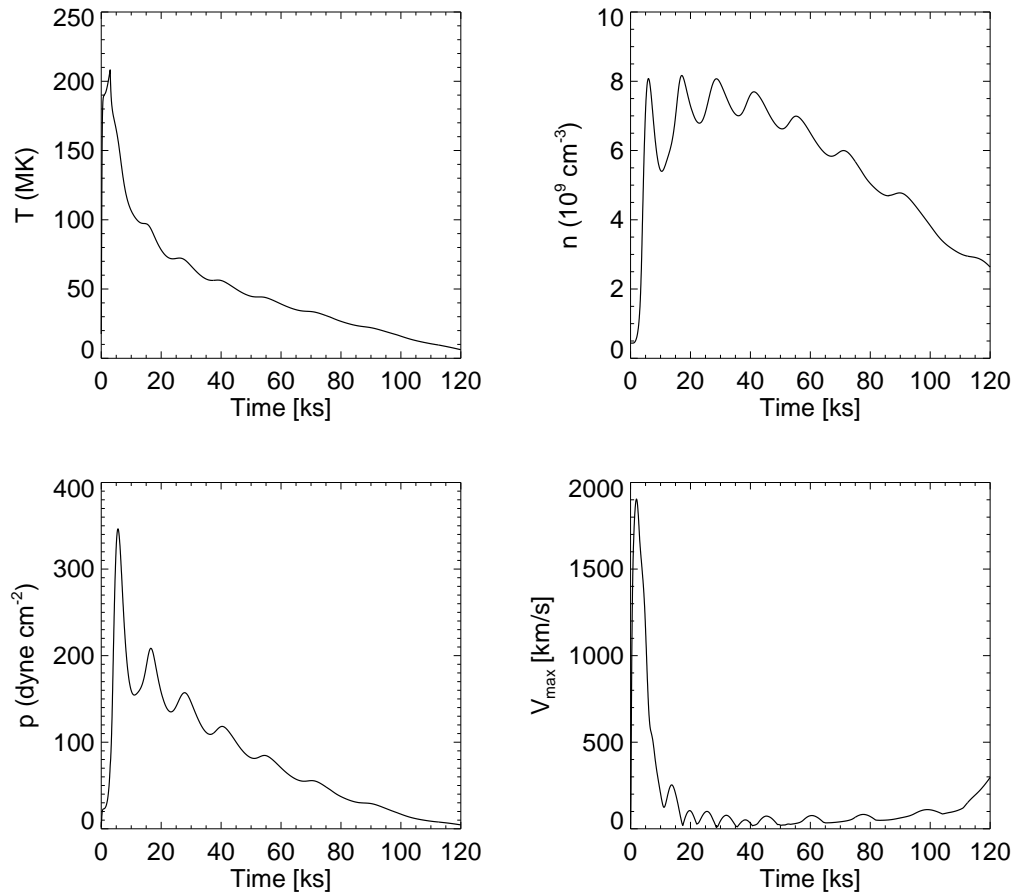


Figure 3. Evolution of the temperature T , density n , pressure p at the middle of the flaring tube, and of the maximum plasma speed V along the tube for the simulation of the flare on V772 Ori.

the middle of the tube, and the maximum absolute speed reached by the plasma along the tube. The temperature rises fast to over 200 MK while the heat pulse is on, and then decreases rapidly and monotonically with an e-folding time $\tau_d \sim 4$ hours, not far from the conduction cooling time (Reale 2014). The pressure and density have a very different evolution. In particular, the density rises more slowly, up to $n \sim 10^{10} \text{ cm}^{-3}$, then it remains relatively steady for about 50 ks and finally decreases gradually.

This overall trend is modulated by well-defined pulsations, similar to those described in a previous work (Reale 2016) and due to plasma sloshing back and forth along the magnetic tube. The period of the pulsations is determined by the sound crossing time during the cooling. In this case, a typical

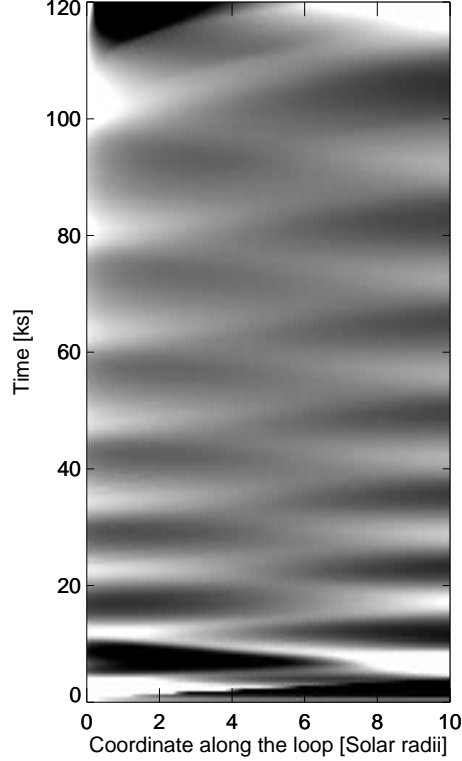


Figure 4. Evolution of the pressure along half of the flux tube from the flare simulation for V772 Ori. The pressure $\pm 20\%$ of the mean at each time is shown. The gray scale is linear (black is low, white is high).

temperature in the decay is ~ 50 MK, which corresponds to $\tau'_s \sim 4$ hours. We see that the period increases with time as expected, because the temperature decreases continuously during the decay. The pressure at mid-point shows a well-defined peak $p_{th} \approx 350$ dyne cm^{-2} at $t \approx 1.5$ hr, and then decreases with periodic pulsations. The velocity shows an initial very high peak of $v_{max} \sim 2000$ km/s due to the explosive expansion of the dense chromospheric plasma upwards into the much more tenuous corona. After this transient, also the velocity oscillates, as the density and pressure. The density and velocity determine the presence of a ram pressure hitting the tube footpoints on the order of $p_{ram} \approx nm_H v^2$, where m_H is the mass of the hydrogen atom. For $n \sim 10^{10}$ cm^{-3} and $v \sim 1000$ km/s, we obtain $p_{ram} \sim 200$ dyne cm^{-2} , i.e., of the same order as the thermal pressure p_{th} estimated above.

As described in [Reale \(2016\)](#), the plasma sloshing is driven by a depression which forms low in the

tube, where the plasma cools more efficiently, as soon as the heat pulse stops. Figure 4 shows the sloshing for this specific situation.

From the density and temperature distribution of the plasma along the model flux tube, we can synthesize the expected plasma X-ray spectrum filtered through the ACIS-I spectral response. We have computed the emission in the coronal part of the flux tube, i.e., above the transition region, as that of an optically thin plasma:

$$I(t) = A \int_L n(t)^2 G[T(t)] dL \quad \text{cts s}^{-1} \quad (4)$$

where t is the time, n is the plasma density, $G(T)$ is the instrumental response function, i.e., the expected count rate spectrum at a temperature T folded through the ACIS-I effective area, integrated over the energy range, and scaled for the star distance, A is the tube cross-section. We assume a hydrogen column density $\log N_H[\text{cm}^{-2}] = 21.2$ and less than solar (0.3) metal abundances (Favata et al. 2005). The photon counts are integrated above 0.4 keV. The tube cross-section is a free parameter that is obtained from scaling the model light curve to the observed one. A good matching is obtained by assuming a circular cross section with a radius $R \approx 0.06 L$, not far from values typical of solar flaring loops ($R/L \sim 0.1$, Golub et al. 1980). This corresponds to a cross-section area of $\sim 10\%$ of the solar surface ($\sim 1\%$ of the actual surface of this star according to known parameters). In this case, for a such a long flux tube, the cross-section might change significantly along the tube and the value we obtain is to be intended as an average. A non-uniform cross-section does not lead to a significant change of the results obtained for a 1D description with uniform cross-section. With this assumption, we obtain an emission measure $\approx 10^{54} \text{ cm}^{-3}$ at the flare peak, in very good agreement with the one diagnosed from the observation (Favata et al. 2005). The maximum temperature in the range 100-150 MK in the flare rise is also in good agreement with the measured effective maximum

temperature between 50 and 100 MK.

From Eq. (4) we derive the light curve shown in Fig. 2 (red solid line); it is not noisy because it is not affected by photon statistics (its sampling time is 500 s, much less than the binnings used for the data in the figure). As a check for consistency, we add Poisson noise to the model count rate and apply the same wavelet analysis as to the real data. Figure 5c shows the light curve with the same binning as the observed one and the related ΔC statistics with respect to the fitted polynomial baseline, to be compared to an observed one (Fig. 5a) among those shown in Fig. 2a. The result of the wavelet analysis with a binning of 100 s is shown in Fig. 5d: we find a strong feature at the long period $P \approx 10$ ks, and in a time range ~ 40 ks, around the peak of the flare, very similar to that detected in the data (Fig. 1). The feature at ~ 30 ks is of short duration, i.e., less than 3 periods, and therefore not relevant in this work. The wave reconstruction (Torrence & Compo 1998; López-Santiago et al. 2016) in Fig. 5b shows data and model oscillations with the same period and amplitude of the same order (within $\sim 30\%$). Note that a non-sinusoidal but periodic signal would produce a wavelet power spectrum very different from that of a sinusoid. For example, the power spectrum of a periodic train of short pulses is revealed in the power spectrum as another pulse train in frequencies, i.e., a vertical feature repeated in time at the position of each pulse. This is not observed in our data. Our data present a wavelet power spectrum typical of damped sinusoids (see Figure 9 of Addison 2016, for an example of an impulse train-like signal).

For completeness, we show also results for a simulation with a heat pulse duration $\tau_H = 10000$ s (≈ 3 hours), i.e., longer than τ_s (Eq.3), deposited in the same magnetic tube. In this case the heat pulse is deposited uniformly along the flux tube with a volume rate $0.05 \text{ erg cm}^{-3} \text{ s}^{-1}$. Figures 6 and 7 show that the overall evolution is very similar to that with the shorter pulse (Figures 3 and 2), except that there is no significant pulsation. This confirms that the pulse duration is critical to reproduce the observed periodic pulsations (Reale 2016). We add Poisson noise to the model light

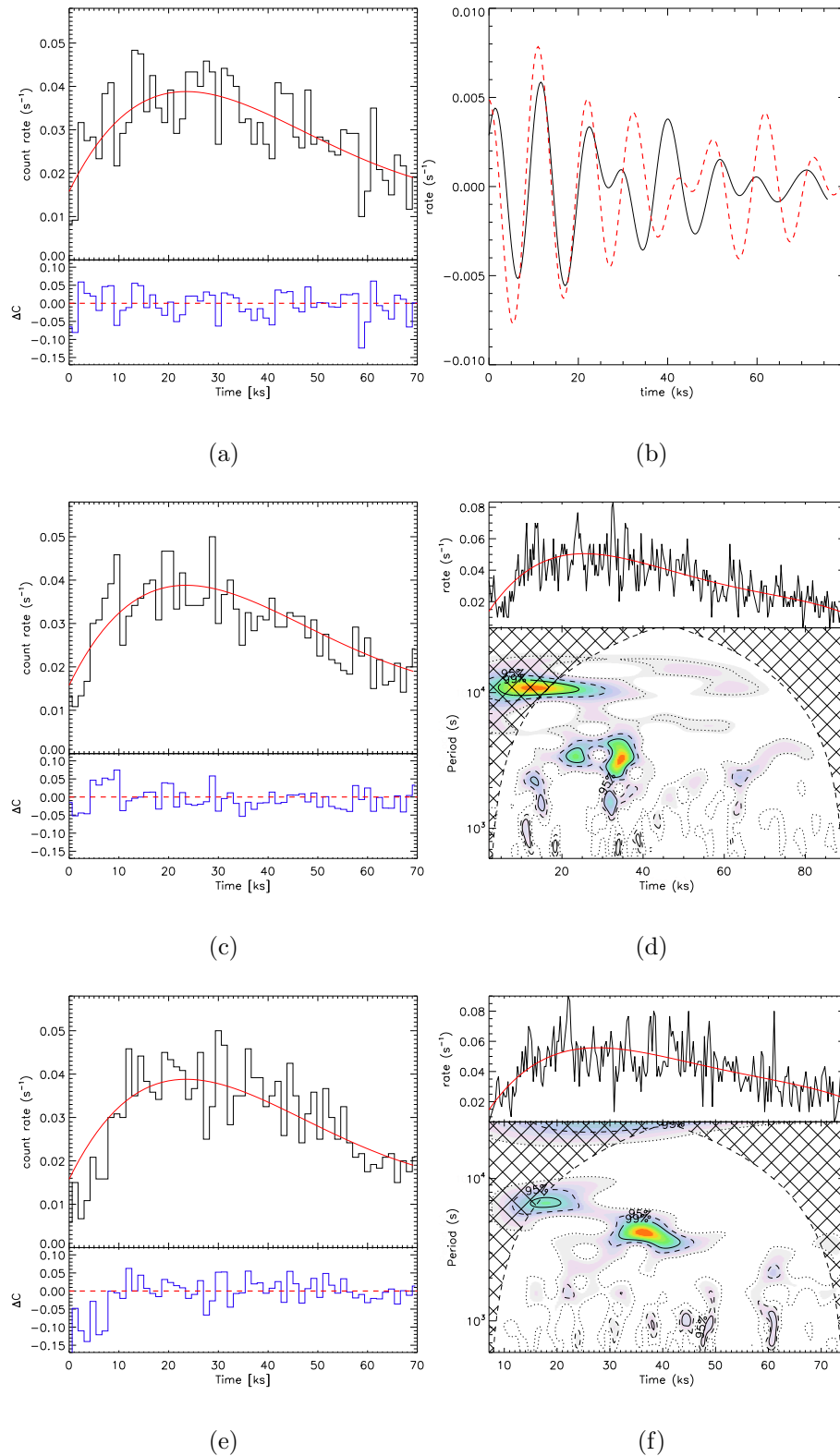


Figure 5. Wavelet analysis of simulated light curves: (a) Observed V772 Ori flare light curve (*histogram*, one of those in Fig. 2a), fitted polynomial baseline (*red line*), and related ΔC statistics. The temporal bin is 1.2 ks. (b) Wave reconstruction from the data (a, *black*) and model (c, *red*). (c,e) Same as (a) synthesized from the HD simulation with and without pulsations, respectively, and including Poisson noise. (d,f) Wavelet power spectrum for the light curves synthesized from the model with (c) and without (e) pulsations, respectively.

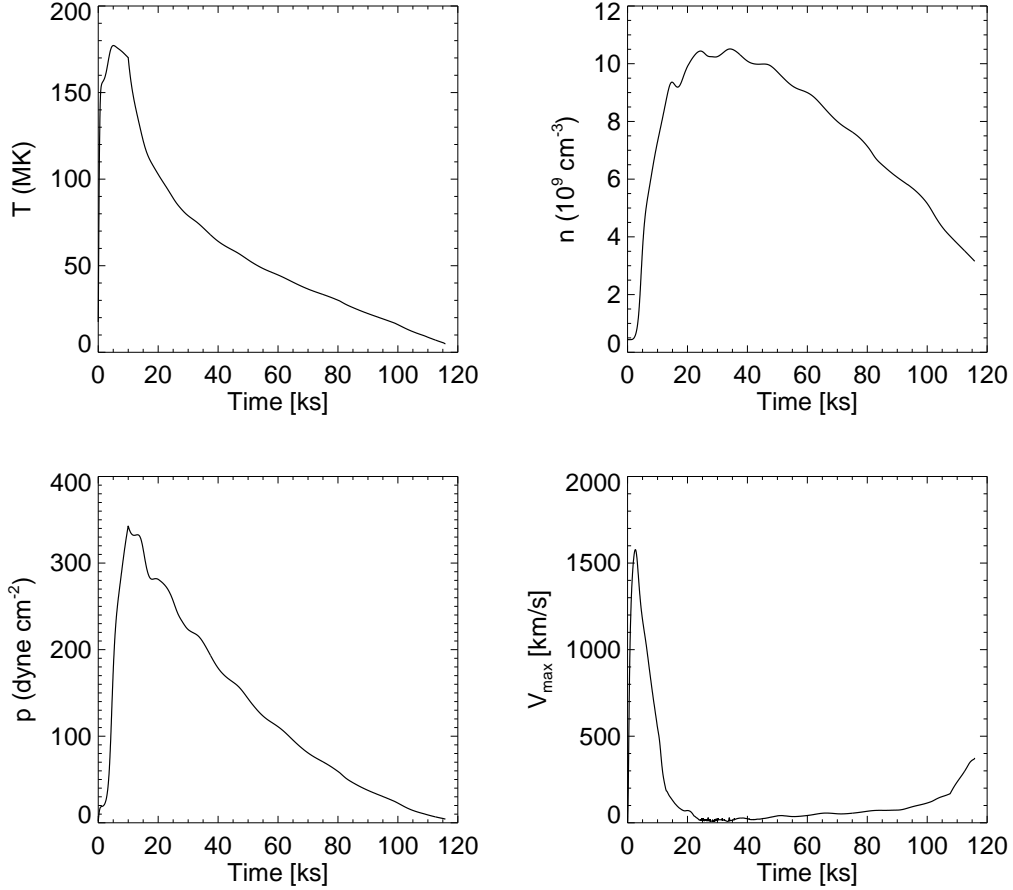


Figure 6. As Figure 3 for a flare simulation with a heat pulse longer than τ_s which does not show pulsations.

curve also for this case (Fig.5e) and apply the wavelet analysis (Fig.5f). The related power spectrum does not show the persistent long-period feature at $P \sim 10$ ks, as expected; the feature at ~ 40 ks is due to a train of tiny ripples (the amplitude is less than 1%), not visible in Fig.7, from small inaccuracies in the calculation of the X-ray emission, and is not of interest for this work. We have also checked that the cross-correlation between the observed and the model light curves grows from 0.53 for the model without oscillations to 0.67 for the model with the oscillations (the threshold for significance is 0.25).

Figure 8 (and Movie 1) shows how the Chandra emission predicted by the model with oscillations is distributed along the possible star-disk connecting flux tube and how it evolves in time during the modelled flare. When integrated along the tube at each time this emission corresponds to the light

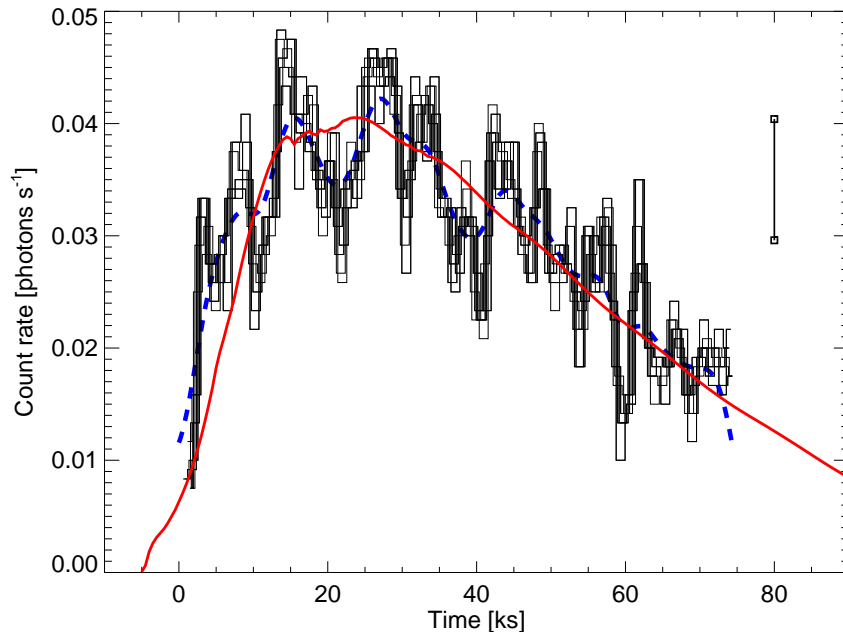


Figure 7. Observed light curve as in Figure 2a (V772 Ori) compared to the one from a simulation with a heat pulse longer than τ_s which does not show pulsations.

curve in Figure 2. A good agreement is obtained by assuming that the tube is 85% visible. Since the plasma is optically thin we expect no other effects due to system inclination.

For the flare on OW Ori, we use the same model and parameters as for the one on V772 Ori, except that the length of the magnetic tube is $L_{\odot} = 28.62$, corresponding to $\sim 16 R_{\star}$. We obtain very similar results and the light curve in Figure 2b is obtained by assuming that the tube is 70% visible.

4. DISCUSSION AND CONCLUSIONS

The light curves in the COUP observation of V772 Ori and OW Ori (Figure 2) show the relatively fast rise and slower decay trend of typical flares, but the wavelet analysis detects that they are modulated by periodic pulsations. The data are compatible with a smooth wave-like modulation. There are two key features in these pulsations: their amplitude is large, i.e. $\sim 10 - 20\%$, and the period is very long, i.e., ~ 3 hours. These features are detected also in other flares on Orion PMS stars (López-Santiago et al. 2016), but in these two flares they are particularly significant.

Quasi-Periodic-Pulsations (QPP) have been extensively observed in flares both on the Sun and on other stars. They have been generally connected to the propagation of waves in the flaring region (Nakariakov & Melnikov 2009; Kumar et al. 2015), but “Despite the many observational and theoretical advances in the last years, it has not been possible to determine what physical mechanism is responsible for causing the QPPs” (Van Doorselaere et al. 2016). The large amplitude makes them difficult to interpret in terms of usual MHD waves or modes. Also the periods of such modes are typically much shorter than those described here (Nakariakov & Melnikov 2009). Very recently, it has been proposed that such pulsations are caused by plasmas sloshing back and forth in closed magnetic tubes triggered by a very short and intense heat pulse (Reale 2016). This model is supported by other works (Su et al. 2012; Fang et al. 2015) and naturally explains the large amplitudes.

Hydrodynamic simulations of the flares along a long magnetic tube at high spatial resolution show that this scenario is able to reproduce the inferred patterns of the light curves. Figures 2 and 5a (red solid lines) show the Chandra/ACIS light curves obtained from the simulation of a flare triggered by a heat pulse with a duration of ~ 1 hour inside magnetic tubes $\approx 20 R_{\odot}$ and $\approx 28 R_{\odot}$ long, respectively, which correspond to $6.7 R_{\star}$ and $16 R_{\star}$ for these stars, respectively (see Section 2).

The heat pulse is spread along the tube which is symmetric with respect to the middle point, and across the tube on an area equivalent to $\sim 10\%$ of the solar surface in both cases. The pulse heats the plasma in the tube rapidly (~ 1 hour) up to a temperature ≥ 200 MK. After the heating is over the plasma rapidly cools down back below 100 MK in about 3 hours, and the cooling continues more gradually for the next several hours. The amount of plasma inside the tube has a slower evolution: dense plasma rises from the tube footpoints initially at supersonic speed (~ 2000 km/s), and takes a couple of hours to fill in the tube completely. Then, the plasma is pulled back by a depression low in the tube and begins to slosh back and forth along the tube. Figure 4 shows the sloshing for V772 Ori. After several hours the plasma starts to drain down and the emission gradually decays.

Since the waves are hydrodynamic and the propagation is sonic, this model does not involve a direct effect of the magnetic field other than that of a waveguide. Because of energy losses, the waves progressively reduce their amplitude and their period becomes longer.

As shown in Figures 2 and 5, this model is able to reproduce both the amplitude and the period of the pulsations of the observed flare light curves. In addition, the model is able to explain at the same time the modulation and the envelope of the light curves (rise and decay) which are ruled by different physical processes, i.e., the sloshing and the heating and cooling, respectively. Two independent lines of reasoning therefore converge to a coherent scenario of a flare in a single and very long magnetic tube, long enough to connect the star to an accretion disk (Hartmann et al. 2016). As customary for time-dependent models, the model does not pretend a perfect match with the observation, because fine-tuning is prohibitive and the data do not allow to resolve enough the fine details of the light curve. Many possible effects simultaneously present, including perturbations, geometric details, and data noise concur to determine the differences. The model reproduces well the pattern, amplitude and period of the pulsations as far as it is allowed by the observation.

Although QPPs are customarily observed in solar flares, the interpretation is not unique. They have already been attributed to episodic outflows (Su et al. 2012), and the model with pulse-driven sloshing is able to explain the pulsations in detail including the large amplitudes (Reale 2016). Similar pulsations have been found also in other numerical loop modeling (Nakariakov et al. 2004; Tsiklauri et al. 2004; Bradshaw & Cargill 2013; Fang et al. 2015). In a more general MHD framework, the sloshing fronts can be viewed as low-order modes of slow magnetosonic waves in a low β plasma. The confinement of the plasma with a pressure of a few hundreds dyne cm^{-2} (Fig. 3) requires a magnetic field of ~ 100 G, which might not be unrealistic even at such large distances from the stellar surface, for stars with average fields of a few kG at the surface (Yang & Johns-Krull 2011). Taken for granted that any kind of fast wave would imply even longer magnetic tubes, it remains the

alternative possibility that the pulsations might mark slow magnetosonic waves in a high β environment. This cannot be completely excluded, although very unlikely because it would imply a strong coherent deformation of the magnetic field, like a fattening or shrinking of the whole tube altogether, not easy to imagine on such huge spatial scales, and also much more energy-demanding.

Our analysis shows that large and slow coherent pulsations in the day-long light curves are explained very well if flaring plasma sloshes back and forth in a single and very long magnetic tube. A multi-loop flare (Warren 2006; Rubio da Costa et al. 2016) is expected to be chaotic and cannot reproduce such simple oscillation patterns, unless coherence is forced by unknown mechanisms. Nothing like this has ever been observed on the Sun, where multiloop flares are frequently observed. Our model naturally reproduces, and quantitatively, both the oscillation pattern and the envelope light curves.

The diagnosed lengths are typical of magnetic tubes connecting the star and the inner disk (Hartmann et al. 2016), as proposed in Figure 8 (see Movie 1). The framework is a young stellar object surrounded by an accretion disk according to an analytical solution (Romanova et al. 2002). For simplicity, the magnetic field is a dipole centered on the star and perpendicular to the plane of symmetry of the disk. The flare X-ray emission is taken from the simulation for V772 Ori and has been mapped along a magnetic tube that links the star to the disk and $\approx 20R_{\odot}$ long. The length of the magnetic tube might easily connect the star to a more distant location on the disk. This distance is well beyond the co-rotation radius, which is $\sim 1.6R_{*}$ for this star. Therefore, the far footpoint is practically at rest with respect to the footpoint on the star. Since the flare duration is a significant fraction of the stellar rotation period ($\sim 180^{\circ}$), one may wonder if the magnetic tube might be significantly stretched during the flare and invalidate the model. However, one footpoint of the tube would be simply dragged along the stellar surface, and therefore the stretching would be of 2 stellar radii at most, only if the footpoint is located at the star equator. If instead it is more likely close to one of the poles, the length would be almost unchanged and the net effect would only be a

twisting of the magnetic channel, which is expected and might even trigger the flare. The model is therefore fully consistent with the geometry and dynamics of the star-disk system.

In the end, this work shows strong evidence that magnetic tubes as long as to connect the star to the circumstellar disk exist and produce flares, and even constrains the heat pulse released in the tube. In such a scenario, flares might play a direct role also in perturbing the circumstellar disks. In addition to obvious strong local ionization and dust destruction due to extremely hot plasma brought close to the disk, the flares produce thermal and ram pressure fronts on the order of some hundreds dyne cm^{-2} (see Section 3), comparable to the internal pressure of T Tauri disks (at an age of $10^5 - 10^6$ yrs) (Ruden & Pollack 1991). By hitting the disk, these fronts would produce significant dynamic perturbations, e.g., warping waves, which might propagate along the disk far from the flare site and influence other processes, including those leading to planet formation. Furthermore, they might themselves trigger accretion episodes, as predicted by detailed MHD modeling (Orlando et al. 2011).

More sensitive observations of flares on PMS stars with forthcoming X-ray missions, such as Athena, will be crucial to better detect this kind of evolution and to shed more light into this scenario.

F.R., E.F., A.P., S.S. acknowledge support from Italian Ministero dell’Istruzione, dell’Università e della Ricerca. J.L.-S. acknowledges the Office of Naval Research Global (award no. N62909-15-1-2011) for support. The research leading to these results has received funding from the European Unions Horizon 2020 Programme under the AHEAD project (grant agreement n. 654215). The authors thank C. Argiroffi and F. Damiani for help.

Software: XSPEC (Schafer 1991), MEKAL (Phillips et al. 1999)

REFERENCES

Aarnio, A. N., Stassun, K. G., & Matt, S. P. 2010, *Astrophys. J.*, 717, 93

Addison, P. S. 2016, *The Illustrated Wavelet Transform Handbook: Introductory Theory and Applications in Science, Engineering, Medicine and Finance* (CRC Press)

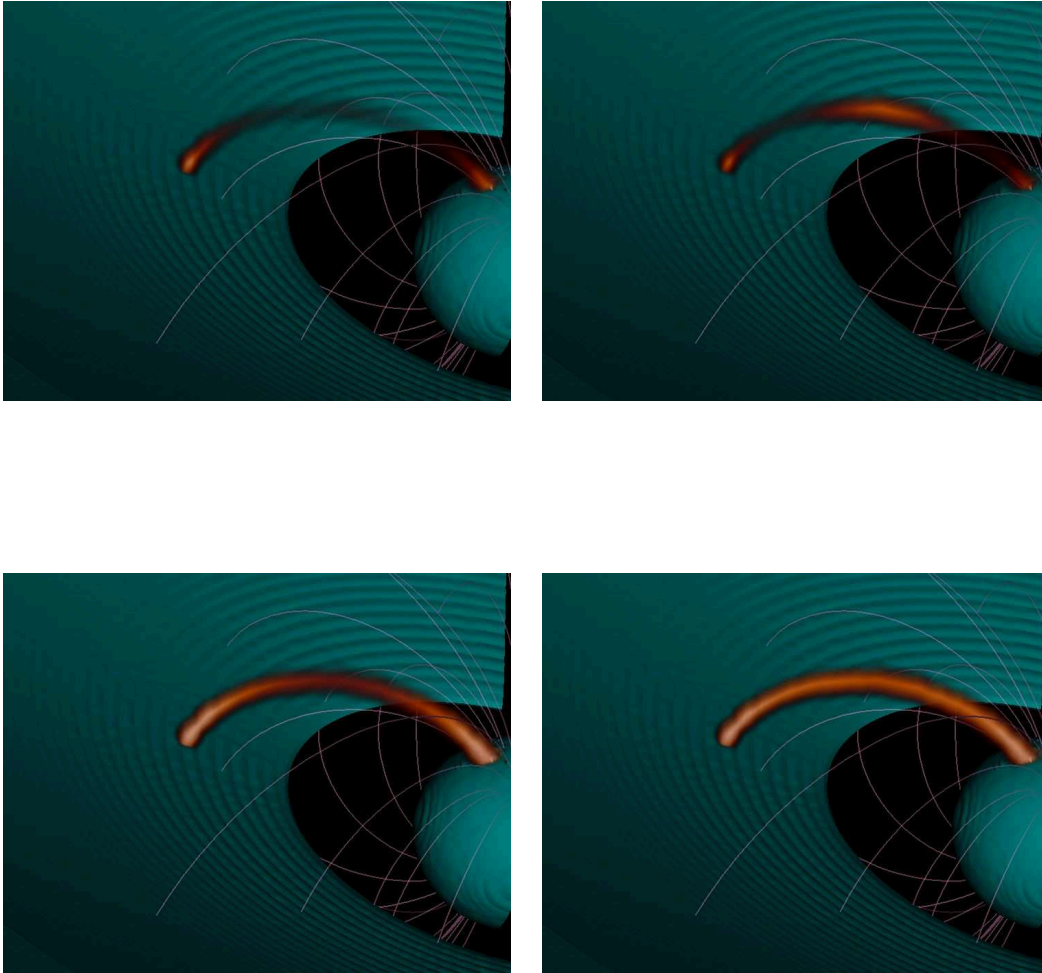


Figure 8. Possible scenario of the flaring magnetic tube in the V772 Ori flare. The framework is a young stellar object surrounded by an accretion disk (green, [Romanova et al. 2002](#)) with a bundle of magnetic field lines (white lines). The flare X-ray emission from the simulation is mapped along a tube around a magnetic field line with a constant cross section (volumetric rendering, linear red scale) that links the star to the disk and $\approx 20R_{\odot}$ long. Each frame shows the X-ray emission detectable with Chandra/ACIS, according to the hydrodynamic simulation shown in Fig. 2. The frames are taken at time 4000 s, 7000 s, 11000 s, and 15000 s since the beginning of the simulation and show the brightness fronts moving back and forth along the tube (see Movie 1 for an animated version of this figure).

- Argiroffi, C., Maggio, A., & Peres, G. 2007, *Astron. Astrophys.*, 465, L5
- Betta, R., Peres, G., Reale, F., & Serio, S. 1997, *Astron. Astrophys. Suppl. Ser.*, 122, 585
- Biazzo, K., Melo, C. H. F., Pasquini, L., et al. 2009, *Astron. Astrophys.*, 508, 1301
- Birk, G. T. 1998, *Astron. Astrophys.*, 330, 1070
- Birk, G. T., Schwab, D., Wiechen, H., & Lesch, H. 2000, *Astron. Astrophys.*, 358, 1027
- Bradshaw, S., & Cargill, P. 2006, *Astron. Astrophys.*, 458, 987
- Bradshaw, S. J., & Cargill, P. J. 2010, *Astrophys. J.*, 717, 163
- . 2013, *Astrophys. J.*, 770, 12
- Fang, X., Yuan, D., Van Doorselaere, T., Keppens, R., & Xia, C. 2015, *Astrophys. J.*, 813, 33
- Favata, F., Flaccomio, E., Reale, F., et al. 2005, *Astrophys. J. Suppl. Ser.*, 160, 469
- Getman, K., Feigelson, E., Micela, G., et al. 2008, *Astrophys. J.*, 688, 437
- Getman, K. V., Feigelson, E. D., Grosso, N., et al. 2005a, *Astron. Astrophys. Suppl. Ser.*, 160, 353
- Getman, K. V., Flaccomio, E., Broos, P. S., et al. 2005b, *Astrophys. J. Suppl. Ser.*, 160, 319
- Giardino, G., Favata, F., Micela, G., Sciortino, S., & Winston, E. 2007, *Astron. Astrophys.*, 463, 275
- Golub, L., Maxson, C., Rosner, R., Vaiana, G., & Serio, S. 1980, *Astrophys. J.*, 238, 343
- Hartmann, L., Herczeg, G., & Calvet, N. 2016, *Annu. Rev. Astron. Astrophys.*, 54, 135
- Hillenbrand, L. A. 1997, *Astronomical J.*, 113, 1733
- Hillenbrand, L. A., Hoffer, A. S., & Herczeg, G. J. 2013, *Astronomical J.*, 146, 85
- Hillenbrand, L. A., Strom, S. E., Calvet, N., et al. 1998, *Astronomical J.*, 116, 1816
- Johns-Krull, C. M. 2014, *Nature*, 514, 571
- Kastner, J. H., Huenemoerder, D. P., Schulz, N. S., Canizares, C. R., & Weintraub, D. A. 2002, *Astrophys. J.*, 567, 434
- Koenigl, A. 1991, *Astrophys. J. Lett.*, 370, L39
- Kounkel, M., Hartmann, L., Loinard, L., et al. 2014, *Astrophys. J.*, 790, 49
- Kumar, P., Nakariakov, V. M., & Cho, K.-S. 2015, *Astrophys. J.*, 804, 4
- López-Santiago, J., Crespo-Chacón, I., Flaccomio, E., et al. 2016, *Astron. Astrophys.*, 590, A7
- Mitra-Kraev, U., Harra, L. K., Williams, D. R., & Kraev, E. 2005, *Astron. Astrophys.*, 436, 1041
- Nakariakov, V. M., & Melnikov, V. F. 2009, *Space Science Reviews*, 149, 119
- Nakariakov, V. M., Tsiklauri, D., Kelly, A., Arber, T. D., & Aschwanden, M. J. 2004, *Astron. Astrophys.*, 414, L25
- Orlando, S., Reale, F., Peres, G., & Mignone, A. 2011, *Mon. Not. R. Astron. Soc.*, 415, 3380
- Pandey, J. C., & Srivastava, A. K. 2009, *Astrophys. J. Lett.*, 697, L153
- Peres, G., Serio, S., Vaiana, G., & Rosner, R. 1982, *Astrophys. J.*, 252, 791
- Phillips, K. J. H., Mewe, R., Harra-Murnion, L. K., et al. 1999, *A&AS*, 138, 381
- Reale, F. 2007, *Astron. Astrophys.*, 471, 271
- Reale, F. 2014, *Living Reviews in Solar Physics*, 11, 4
- . 2016, *Astrophys. J. Lett.*, 826, L20
- Reale, F., Betta, R., Peres, G., Serio, S., & McTiernan, J. 1997, *Astron. Astrophys.*, 325, 782
- Reale, F., Peres, G., Serio, S., Rosner, R., & Schmitt, J. 1988, *Astrophys. J.*, 328, 256
- Reale, F., Parenti, S., Reeves, K., et al. 2007, *Science*, 318, 1582
- Rhode, K. L., Herbst, W., & Mathieu, R. D. 2001, *Astronomical J.*, 122, 3258
- Romanova, M. M., Ustyugova, G. V., Koldoba, A. V., & Lovelace, R. V. E. 2002, *Astrophys. J.*, 578, 420
- Rosner, R., Tucker, W., & Vaiana, G. 1978, *Astrophys. J.*, 220, 643
- Rubio da Costa, F., Kleint, L., Petrosian, V., Liu, W., & Allred, J. C. 2016, *Astrophys. J.*, 827, 38
- Ruden, S. P., & Pollack, J. B. 1991, *Astrophys. J.*, 375, 740
- Schafer, R. A. 1991, XSPEC, an x-ray spectral fitting package : version 2 of the user's guide
- Schmitt, J. H. M. M., Reale, F., Liefke, C., et al. 2008, *Astron. Astrophys.*, 481, 799
- Serio, S., Reale, F., Jakimiec, J., Sylwester, B., & Sylwester, J. 1991, *Astron. Astrophys.*, 241, 197
- Stassun, K. G., Mathieu, R. D., Mazeh, T., & Vrba, F. J. 1999, *Astronomical J.*, 117, 2941
- Su, J. T., Shen, Y. D., & Liu, Y. 2012, *Astrophys. J.*, 754, 43
- Telleschi, A., Güdel, M., Briggs, K. R., Audard, M., & Scelsi, L. 2007, *Astron. Astrophys.*, 468, 443
- Testa, P., Reale, F., Garcia-Alvarez, D., & Huenemoerder, D. P. 2007, *Astrophys. J.*, 663, 1232
- Torrence, C., & Compo, G. P. 1998, *Bulletin of the American Meteorological Society*, 79, 61
- Tsiklauri, D., Nakariakov, V. M., Arber, T. D., & Aschwanden, M. J. 2004, *Astron. Astrophys.*, 422, 351
- Van Doorselaere, T., Kupriyanova, E. G., & Yuan, D. 2016, *Solar Phys.*, 291, 3143
- Vernazza, J., Avrett, E., & Loeser, R. 1981, *Astrophys. J. Suppl. Ser.*, 45, 635
- Warren, H. 2006, *Astrophys. J.*, 637, 522
- Welsh, B. Y., Wheatley, J., Browne, S. E., et al. 2006, *Astron. Astrophys.*, 458, 921
- Yang, H., & Johns-Krull, C. M. 2011, *Astrophys. J.*, 729, 83